Effect of Debonding on Overall Behavior of AA3003/Titanium Carbide Nanoparticulate Reinforced Metal Matrix Composites

[1]B. Kotiveera Chari and A. Chennakesava Reddy[2]

[1]Professor, Department of Mechanical Engineering, NIT, Warangal, India
[2]Assistant Professor, Department of Mechanical Engineering, MJ College of Engineering and Technology, Hyderabad, India
dr_acreddy@yahoo.com

Abstract: A diamond array unit cell/2-D rhombus particulate RVE models were employed to predict interfacial debonding using cohesive zone analysis. The particulate metal matrix composites are titanium carbide/AA3003 alloy at different volume fractions of titanium carbide. Interface debonding was observed in all the composites. The traction increases with separation reaches a maximum and subsequently subsides to zero traction, signaling debonding.

Keywords: AA3003, titanium carbide, rhombus particulate, RVE model, finite element analysis, interface debonding.

1. INTRODUCTION

The micro-mechanisms of failure in particulate metal matrix composite materials involve either particulate fracture or particulate-matrix interface decohesion, followed by matrix cracking. The damage mechanisms are sensitive to local morphological parameters like volume fraction, size, shape and spatial distribution of reinforcements, interfacial strength and process-related defects. The effect of weak bonding or debonded interface on the mechanical properties has been studied by several investigators using simplified models for representing imperfect conditions through traction discontinuities [1-3]. The propagation of interfacial cracking or decohesion at particulate-matrix interfaces has been successfully modeled by a number of researchers using the cohesive volumetric finite element methods [4-18].

In the present research, interfacial debonding analysis was carried out using cohesive zone models in AA3003/titanium carbide nanoparticulate-reinforced metal matrix composites. Representative volume elements (RVEs) models were taken from the periodic 2-D rhombus particulates in a diamond array distribution.

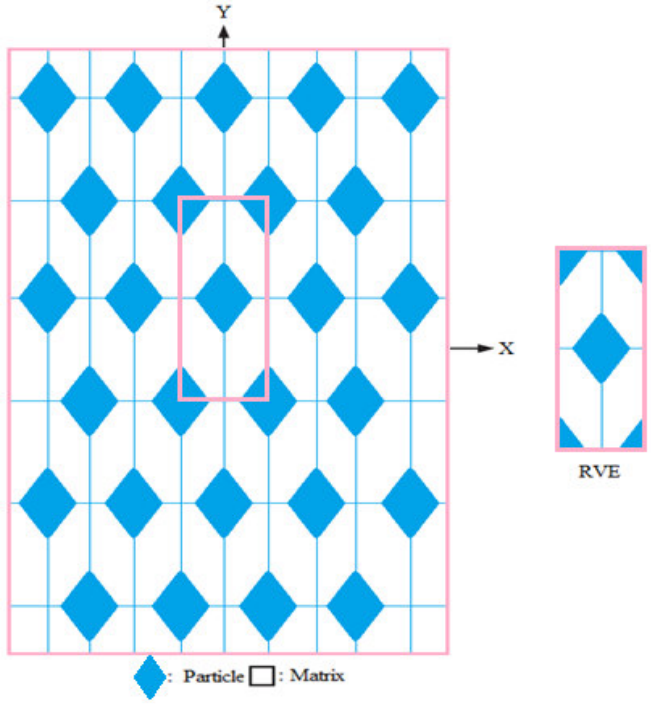

Figure 1: The RVE model.

2. MATERIALS AND METHODS

The volume fractions of titanium carbide used in the present work were 10%, 20%, and 30%. The matrix material was AA3003 alloy. The periodic model for the representative volume element (RVE) scheme was constructed from 2-D rhombus particulates in a diamond array particulate distribution (figure 1). PLANE183 element was used for the matrix and the nanoparticulates. The cohesive zone can be incorporated in the continuum formulation by applying the cohesive tractions as boundary conditions. The cohesive element is implemented as a linear element with four nodes.

Shear-log model is based on the assumption that all of the load transfer from matrix to particulate occurs via shear stresses acting on the particulate interface between the two constituents. The rate of change of the stress in the particulate to the interfacial shear stress at that point and the particulate radius, 'r' is given by:

$$\frac{d\sigma_p}{dx} = -\frac{2\tau_i}{r} \quad (1)$$

which may be regarded as the basic shear lag relationship.

The stress distribution in the particulate is determined by relating shear strains in the matrix around the particulate to the macroscopic strain of the composite. Some mathematical manipulation leads to a solution for the distribution of stress at a distance 'x' from the mid-point of the particulate which involves hyperbolic trig functions:

$$\sigma_p = E_p \varepsilon_c [1 - cosh(nx/r) sech(ns)] \quad (2)$$

where ε_c is the composite strain, s is the particulate aspect ratio (length/diameter) and n is a dimensionless constant given by:

$$n = \left[\frac{2E_m}{E_p(1+v_m)ln(1+v_p)}\right]^{1/2} \quad (3)$$

in which v_m is the Poisson ratio of the matrix. The variation of interfacial shear stress along the particulate length is derived, according to Equation (1), by differentiating this equation, to give:

$$\tau_i = \frac{n\varepsilon_c}{2} E_p sinh\left(\frac{nx}{r}\right) sech(ns) \quad (4)$$

The equation for the stress in the particulate, together with the assumption of a average tensile strain in the matrix equal to that imposed on the composite, can be used to evaluate the composite stiffness. This leads to:

$$\sigma_c = \varepsilon_c \left[v_p E_p \left(1 - \frac{tanh(ns)}{ns}\right) + (1 - v_p) E_m\right] \quad (5)$$

The expression in square brackets is the composite stiffness. The stiffness is a function of particulate aspect ratio, particulate/matrix stiffness ratio and particulate volume fraction.

If the particle deforms in an elastic manner (according to Hooke's law) then,

$$\tau = \frac{n}{2}\sigma_p \quad (6)$$

If interfacial debonding/yielding is considered to occur when the interfacial shear stress reaches its shear strength

$$\tau = \tau_{max} \quad (7)$$

For particle/matrix interfacial fracture can be established whereby,

$$\tau_{max} < \frac{n\sigma_p}{2} \quad (8)$$

This approach suggests that the outcome of a matrix crack impinging on an embedded particle depends on the balance between the particle strength and the shear strength of the interface. For plane strain conditions, the macro stress- macro strain relation is as follows:

$$\begin{Bmatrix} \overline{\sigma_x} \\ \overline{\sigma_y} \\ \overline{\tau_{xy}} \end{Bmatrix} = \begin{bmatrix} \overline{C_{11}} & \overline{C_{12}} & 0 \\ \overline{C_{21}} & \overline{C_{22}} & 0 \\ 0 & 0 & \overline{C_{33}} \end{bmatrix} \times \begin{Bmatrix} \overline{\varepsilon_x} \\ \overline{\varepsilon_y} \\ \overline{\gamma_{xy}} \end{Bmatrix} \quad (9)$$

The interfacial tractions can be obtained by transforming the micro stresses at the interface as given in Eq. (3):

$$t = \begin{Bmatrix} t_z \\ t_n \\ t_t \end{Bmatrix} = T\sigma \quad (10)$$

where, $T = \begin{bmatrix} 0 & 0 & 0 \\ cos^2\theta & sin^2\theta & 2sin\theta cos\theta \\ -sin\theta cos\theta & sin\theta cos\theta & cos^2\theta - sin^2\theta \end{bmatrix}$

3. RESULTS AND DISCUSSION

The tensile modulus and compressive modulus decreased with volume fraction of titanium carbide as shown figure 2a. The shear modulus and major Poisson's ratio also decreased with increase in the volume fraction of titanium carbide in the

composites (figure 2b and 2c). The difference in the elastic moduli of titanium carbide particulates and AA3003 alloy matrix is 331.10 GPa. The Poisson's ratios of AA3003 alloy matrix and titanium carbide particulates are, respectively, 0.33 and 0.19. The condition $\tau_{max} < n\sigma_p/2$ satisfied for the occurrence of debonding in the composites including 10%, 20% and 30% titanium carbide (figure 3). The shear stresses induced in the composites are shown in figure 4. The von Mises stresses induced (figure 4) in titanium particulates are higher than the shear stresses induced at the interfaces.

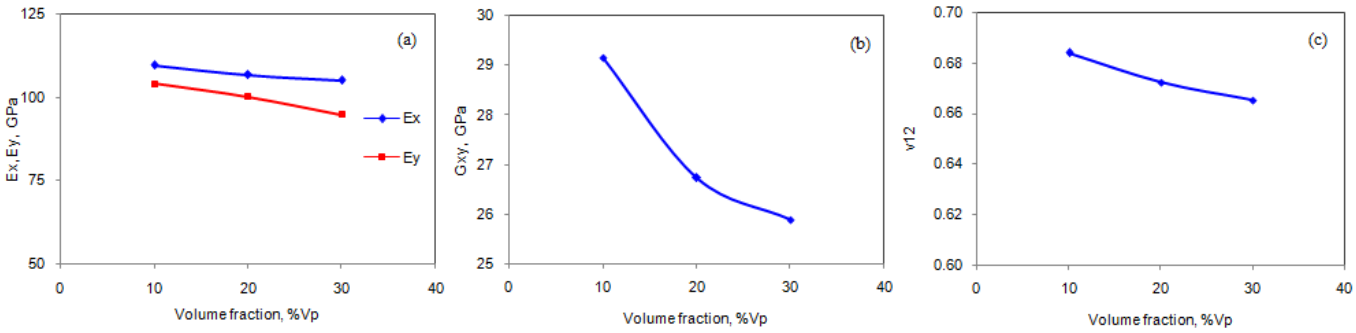

Figure 2: Effect of volume fraction on effective material properties.

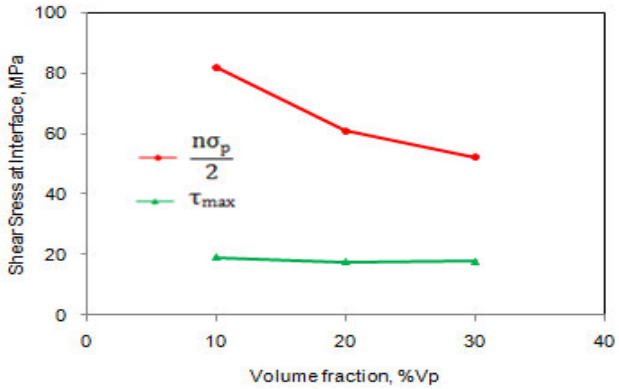

Figure 3: Fracture criteria of interface debonding.

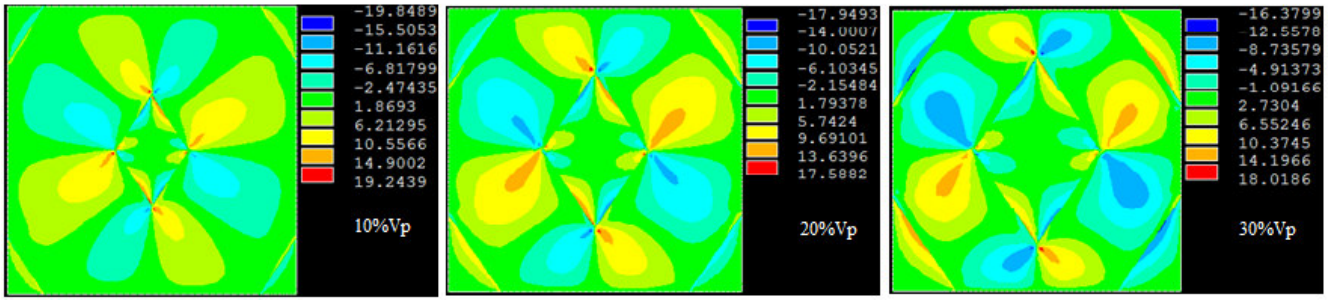

Figure 4: Effect of volume fraction on shear strength.

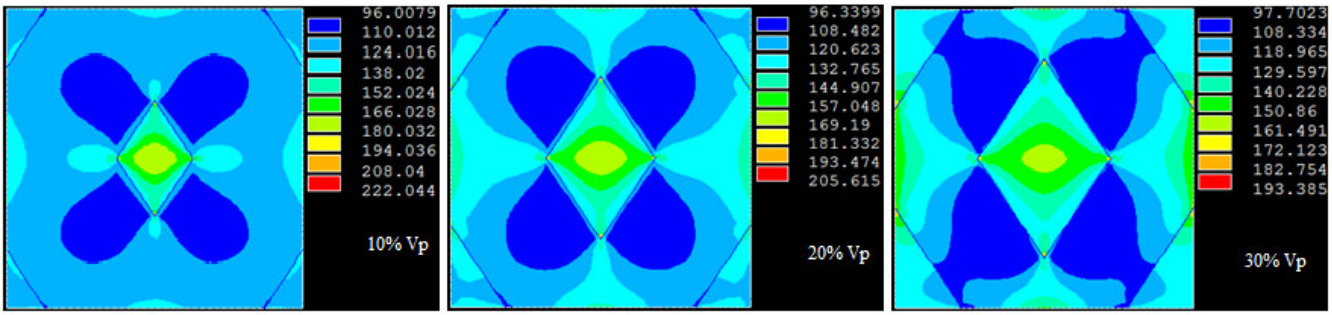

Figure 5: Effect of volume fraction on von Mises stress.

The normal and tangential tractions are plotted in figure 6a. Because of symmetry considerations, the variations of the interface stresses with circumferential location are plotted only for the range $0^o \le \theta \le 90^o$. For AA3003/10%titanium carbide composites, the normal tractions are higher than that for AA3003/20% titanium carbide and AA3003/30% titanium carbide composites. The interface debonding occurred between $0^o \le \theta \le 60^o$. The normal and tangential displacements are also plotted in figure 6b. The normal and tangential displacements are higher for AA3003/10% titanium carbide composites than those for AA3003/20% titanium carbide and AA3003/30% titanium carbide composites. The interfacial response is described by constitutive relations that prescribe the dependence of interface tractions on interfacial separation. It should be noted that the interfacial zone has zero thickness prior to deformation, but nodes may separate with progression of deformation. Traction across the interface reaches a maximum, subsequently decreases and eventually vanishes with increasing interfacial separation, signaling complete debonding. The cohesive zone parameters are σ_{max}, the maximum traction carried by the interface undergoing a purely normal separation (zero displacement).

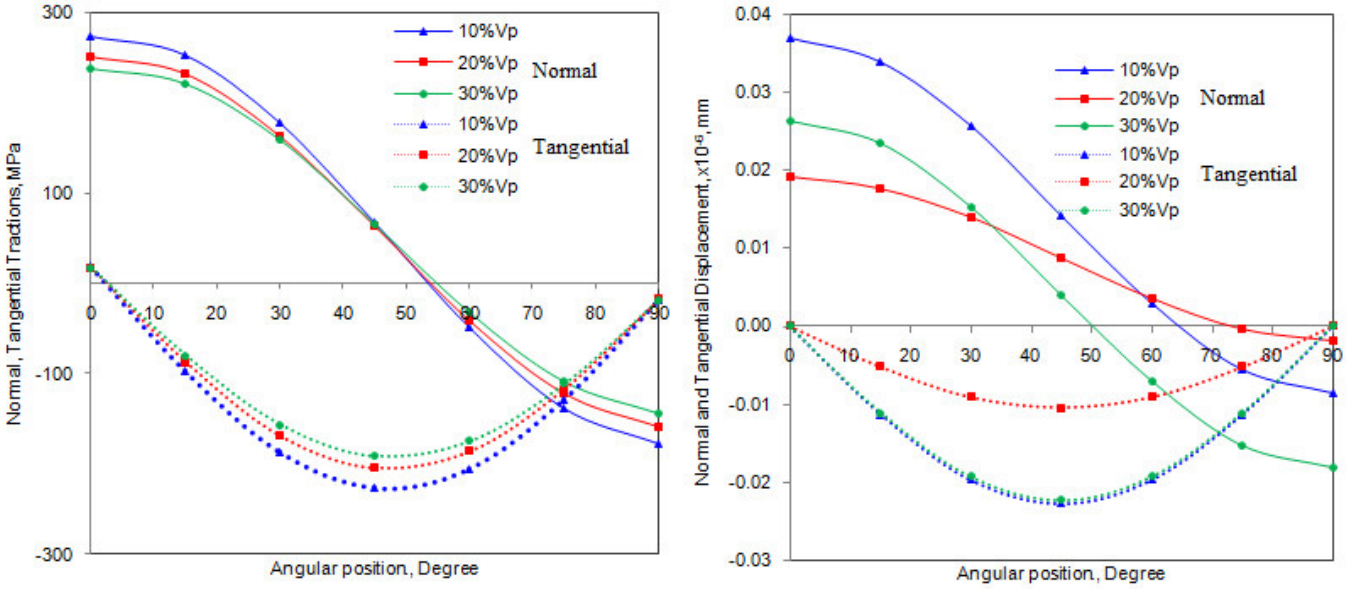

Figure 6: Normal and tangential: (a) tractions and (b) displacements.

4. CONCLUSION

The interface debonding occurred in the composites containing 10%, 20% and 30% volume fractions titanium carbide. The progress of interfacial debonding with quasi-static loading is modeled by cohesive zone constitutive relations in terms of normal and tangential tractions and interfacial separation. In these relations, the traction increases with separation reaches a maximum and subsequently subsides to zero traction, signaling debonding.

REFERENCES

1. Y. Benveniste, On the effect of debonding on the overall behavior of composite materials, Mechanics of Materials, 3, 1984, pp. 349-358.
2. Z. Hashin, Thermoelastic properties of fiber composites with imperfect interface, Mechanics of Materials, 8,, 1990, pp. 333-348.
3. N. J. Pagano, G. P. Tandon, Modeling of imperfect bonding in fiber reinforced brittle matrix composites. Mechanics of Materials, 9, 1990, pp. 49-64.
4. A. Needleman, An analysis of decohesion along an imperfect interface. International Journal of Fracture, 42, 1990, pp. 21-40.
5. A. Chennakesava Reddy, Assessment of Debonding and Particulate Fracture Occurrences in Circular Silicon Nitride Particulate/AA5050 Alloy Metal Matrix Composites , National Conference on Materials and Manufacturing Processes, Hyderabad, India, 27-28 February1998, pp.104-109.
6. B. Kotiveera Chari and A. Chennakesava Reddy, Numerical Simulation of Particulate Fracture in Round Silicon Nitride Particulate/AA6061 Alloy Metal Matrix Composites, National Conference on Materials and Manufacturing Processes, Hyderabad, India, 27-28 February 1998, pp. 110-114.
7. H. B. Niranjan and A. Chennakesava Reddy, Effect of Elastic Moduli Mismatch on Particulate Fracture in AA7020/Silicon Nitride Particulate Metal Matrix Composites , National Conference on Materials and Manufacturing Processes, Hyderabad, India, 27-28 February, 1998, pp. 115-118,

8. P. Martin Jebaraj and A. Chennakesava Reddy, Cohesive Zone Modelling for Interface Debonding in AA8090/Silicon Nitride Nanoparticulate Metal Matrix Composites, National Conference on Materials and Manufacturing Processes, Hyderabad, India, 27-28 February 1998, pp. 119-122.
9. P. Martin Jebaraj and A. Chennakesava Reddy, Plane Strain Finite Element Modeling for Interface Debonding in AA1100/Silicon Oxide Nanoparticulate Metal Matrix Composites, National Conference on Materials and Manufacturing Processes, Hyderabad, India, 27-28 February 1998, pp. 123-126.
10. A. Chennakesava Reddy, Local Stress Differential for Particulate Fracture in AA2024/Titanium Carbide Nanoparticulate Metal Matrix Composites, National Conference on Materials and Manufacturing Processes, Hyderabad, India, 27-28 February 1998, pp. 127-131.
11. B. Kotiveera Chari and A. Chennakesava Reddy, Interface Debonding and Particulate Facture based on Strain Energy Density in AA3003/MgO Nanoparticulate Metal Matrix Composites, National Conference on Materials and Manufacturing Processes, Hyderabad, India, 27-28 February 1998, pp. 132-136.
12. H. B. Niranjan and A. Chennakesava Reddy, Numerical and Analytical Prediction of Interface Debonding in AA4015/Boron Nitride Nanoparticulate Metal Matrix Composites , National Conference on Materials and Manufacturing Processes, Hyderabad, India, 27-28 February 1998, pp. 137-140.
13. S. Sundara Rajan and A. Chennakesava Reddy, Effect of Particulate Volume Fraction on Particulate Cracking in AA5050/Zirconium Oxide Nanoparticulate Metal Matrix Composites , National Conference on Materials and Manufacturing Processes, Hyderabad, India, 27-28 February 1998, pp. 156-159.
14. S. Sundara Rajan and A. Chennakesava Reddy, Cohesive Zone Analysis for Interface Debonding in AA6061/Titanium Nitride Nanoparticulate Metal Matrix Composites , National Conference on Materials and Manufacturing Processes, Hyderabad, India, 27-28 February 1998, pp. 160-164.
15. A. Chennakesava Reddy, Effect of Particle Loading on Microealstic Behavior and interfacial Tractions of Boron Carbide/AA4015 Alloy Metal Matrix Composites, 1st International Conference on Composite Materials and Characterization, Bangalore, 14-15 march 1997, pp. 176-179.7
16. A. Chennakesava Reddy, Reckoning of Micro-stresses and interfacial Tractions in Titanium Boride/AA2024 Alloy Metal Matrix Composites, 1st International Conference on Composite Materials and Characterization, Bangalore, 14-15 march 1997, pp. 195-197.
17. A. Chennakesava Reddy, Interfacial Debonding Analysis in Terms of Interfacial Tractions for Titanium Boride/AA3003 Alloy Metal Matrix Composites, 1st National Conference on Modern Materials and Manufacturing , Pune, India, 19-20 December 1997, pp. 124-127.
18. A. Chennakesava Reddy, Evaluation of Debonding and Dislocation Occurrences in Rhombus Silicon Nitride Particulate/AA4015 Alloy Metal Matrix Composites, 1st National Conference on Modern Materials and Manufacturing , Pune, India, 19-20 December 1997, pp. 278-282.